

Reactive ion-atom collisions in cw-laser photoionization of laser-cooled Rb atoms

Wei-Chen Liang^{1†}, Feng-Dong Jia^{1†}, Fei Wang², Xi Zhang¹, Yu-Han Wang¹, Jing-Yu Qian¹, Jin-Yu Zhou¹, Yong Wu³, Jian-Guo Wang³, Ping Xue² and Zhi-Ping Zhong^{1,4*}

¹School of Physical Sciences, University of Chinese Academy of Sciences, Beijing, 100049, Beijing, People's Republic of China.

²State Key Laboratory of Low-Dimensional Quantum Physics and Department of Physics, Tsinghua University, Beijing, 100084, Beijing, People's Republic of China.

³Institute of Applied Physics and Computational Mathematics, Beijing, 100088, Beijing, People's Republic of China.

⁴CAS Center for Excellence in Topological Quantum Computation, University of Chinese Academy of Sciences, Beijing, 100190, Beijing, People's Republic of China.

*Corresponding author(s). E-mail(s): zpzhong@ucas.ac.cn;

Contributing authors: liangweichen20@mails.ucas.ac.cn;
fdjia@ucas.ac.cn; f-wang22@mails.tsinghua.edu.cn;
zhangxi191@mails.ucas.ac.cn; wangyuhan21@mails.ucas.ac.cn;
qianjingyu19@mails.ucas.ac.cn; 10175300214@stu.ecnu.edu.cn;
wu_yong@iapcm.ac.cn; wang_jianguo@iapcm.ac.cn;
xuep@tsinghua.edu.cn;

[†]These authors contributed equally to this work.

Abstract

Low-energy ion-atom reactive collision enables precise observation of chemical reactions and the discovery of novel chemical dynamics. Given the importance of such reactions in the chemistry of the interstellar medium, which provides the raw materials for the formation of stars, planets, and possibly even life, understanding these reactions at low temperatures is a fundamental goal for chemistry and physics.

Here, we experimentally studied ion-atom reactive collisions and its dynamics by photoionizing cold rubidium atoms based on an ion-atom hybrid trap. Through manipulating the start-stop of reactive collisions and using time-of-flight mass spectrometry, we directly measured evolution of yield, temperature as well as lifetime of reaction products, e.g., Rb_2^+ and Rb_3^+ molecular ions during photoionization. A well-fitting rate-equation model was established by modelling the experiments. Accordingly, we had obtained of two-body Rb-Rb^+ and Rb-Rb_2^+ reaction-rate coefficients and ion diffusion rate. Our measured ion diffusion rate has manifested electrons' effect on reactive collisions. The obtained reaction rates Rb-Rb^+ reaction rate agrees with classical Langevin model while Rb-Rb_2^+ reaction rate is smaller than Langevin prediction. And we had founded that the lifetime of products extends through vibrational quenching and is anticorrelated to collision energy E_{col} of ion-atom reactions in mK-K regime. Moreover, we observed long-lived temperature relaxation in a multispecies ionic mixture, extending the understand of non-equilibrium transport properties in a Coulomb mixture. Our work manifests a powerful toolbox for studying reactive ion-atom collisions, paving the way for the study of complex many-body systems and tunable inter-particle interactions.

Keywords: Ion-atom reactive collision, Reaction-rate coefficient, Lifetime of reaction products, Temperature relaxation

Over the past two decades, the uprising cold hybrid ion-atom systems has made tremendous progress in studying inelastic collisions and reactions. While early research focused on all-neutral chemistry, recent interests had been a shift to the study of charged-neutral reactions[1–5] as available techniques allow for the probing of a broader range of energy and species[6–8], as well as trapping and studying reaction products[9, 10]. As one of the exotic products of ion-atom chemical reactions, triatomic molecular ions H_3^+ is the most abundant charged molecules among the universe, playing a crucial role in the early astrochemistry responsible for the formation of stars[11]. As hydrogen like species, alkali atoms and ions share a lot of characteristics with hydrogen atom and ions. The existence of H_3^+ suggests the presence of alkali metal X_3^+ molecular ions, whose possibility has been theoretically verified[12]. With the interaction potential following $V(r) \propto -1/r^4$ (r is the internuclear distance), there is also expected to have a large reaction cross section between diatomic molecular ions and atoms[12, 13]. This suggests the experimental investigation and application of alkali metal X_3^+ should be possible in experiments with cold ion-atom mixtures. While studies on reactive collisions between molecular ions and atoms have been presented[12–14], no experimental observation of alkali metal X_3^+ molecular ions has been reported yet, nor the measurement of reaction rates and other kinetic properties.

As the most important physical quantity in a reaction, the chemical reaction rates is significant for almost all applications. It is the key to achieve

the technique of precisely controlling the reaction process to obtain different product branching ratios by different reaction mechanisms[15]. Currently, reactive two-body collision coefficients or cross section for atomic ion-atom systems are only reported experimentally for alkaline earth-ion, and alkaline earth- or alkali metal-heteronuclear systems[1, 2, 16–24]. The difference in reactive collision rate coefficients for alkaline earth-ion, and alkaline earth- or alkali metal-heteronuclear systems varies in a wide range 10^{-10} cm³/s to 10^{-13} cm³/s[1, 2, 17–19, 21, 22, 24]. As for the homonuclear systems, no two-body reaction rate coefficient has yet been reported. Moreover, in most of these studies, ion-atom reaction rate coefficients are generally determined by the information on reactants rather than products because direct measurement of reaction products require a large ensemble of products or advanced technique, either of which is difficult to achieve experimentally until recent[16, 23, 25]. Dieterle *et al.*[16, 23] had used time-of-flight mass spectrometry (TOF-MS) to directly measure the yield of molecular ions and obtained three-body reaction rates. However, their TOF spectrum was not able to record temperature or kinetic energy of ions because they were using a single-ion ensemble. Because previous studies on ion-atom reactions only gave limited information, the subsequent kinetics of reaction products after reactive collisions is largely remain unknown[23, 24].

In this Article, we advanced the study of ion-atom reactive collisions by continuously photoionizing rubidium atoms in an ion-atom hybrid trap. Our apparatus enables us to precisely control the start-stop of reactive collisions and directly measuring reaction products by time-of-flight mass spectrometry. Accordingly, we had directly observed Rb_3^+ and Rb_2^+ molecular ions as products of Rb-Rb_2^+ and Rb-Rb^+ reactions, respectively and measured the evolution of yield, temperature and lifetime of reactants and products during the photoionization. Then, a well-fitting rate-equation model was established and Rb-Rb_2^+ and Rb-Rb^+ reaction-rate coefficients and ion diffusion rate were obtained through fitting the experimental data. Specifically, measured Rb-Rb^+ reaction-rate coefficient well matches the prediction of classical Langevin model[13, 26], while measured Rb-Rb_2^+ reaction rate is smaller than the Langevin prediction. And the measured ion diffusion rate has shown the effect of electrons on reactive collisions. Besides, measurement on the evolution of lifetime of products suggested that the quantum state of products is affected by the competition between vibrational quenching effect[14] and the increase of collision energy. Moreover, we observed a long-lived temperature relaxation of ionic mixture, extending the understanding non-equilibrium Coulomb systems. These results has provided a novel aspect of understanding the dynamics in ion-atom reactive collisions, revealing new possibilities to test fundamental physics and chemistry, precisely manipulate inter-particle interactions and various other applications.

Our experiments are conducted in an Rb^+ -Rb hybrid trap[7], which comprises an Rb standard magneto-optical trap (MOT) for atoms and a mass-selective linear Paul trap (LPT) for ions. The MOT and ion trap are spatially

concentric and combined in a polyhedral flat non-magnetic stainless-steel cavity. In a typical experimental cycle, cold Rb atoms were firstly loaded into the MOT until atomic number is stable. Then, Rb^+ ions were produced by the two-step cw-laser photoionization and trapped in the LPT simultaneously. The first excitation laser was the MOT cooling laser with a detuning of 12 MHz of the transition $5^2S_{1/2}, F = 2 \rightarrow 5^2P_{3/2}, F' = 3$. The second excitation laser, that is, ionization laser, was provided by another cw-diode laser. The ionizing laser and LPT were kept on for a predetermined duration that allows continuously photoionization of atoms and constant presence of ion-atom reactive collisions. After the photoionization period, the ionizing laser, MOT and LPT were simultaneously switched off. Then number and density of atoms were measured by absorption imaging and a time-of-flight mass spectrometer (TOF-MS) was used to collect information of the ionic mixture containing products and reactants. Specifically, ions was counted by a multichannel plate (MCP) detector by switching off the voltage on the end-cap ring electrode closer to the MCP, then trapped ions were pushed to the MCP and TOF spectrum of the ions was recorded by an oscilloscope[7]. In each experimental cycle, we change the duration of photoionization. As a result, information on atoms and ions as a function of photoionization duration was recorded. In order to distinguish different ion species, we applied a extra weak RF field on the quadrupole rods of ion trap. By setting the frequency of this RF field to resonant frequency of radial micromotion of specified ions, these ions would be rapidly heated and escaped from the ion trap[27]. As shown in Fig.1, after 10 ms of heating duration, when frequency of this RF field varied from 5 kHz to 20 kHz, three distinguished peaks respectively showed up in the TOF spectrum, suggesting three species with different charge-to-mass ratio. Considering only Rb atoms and ions existed in our system, the three peaks should correspond to Rb^+ , Rb_2^+ and Rb_3^+ , respectively as time-of-flight increasing.

In our experiments, system parameters are given as follows. The number of atoms and $1/e^2$ half-waist of the cold atomic cloud in MOT were measured as $5 \sim 10 \times 10^7$, $0.5 \sim 1.0$ mm using absorption imaging[28] and the temperature T of atoms was approximately 200μ K. The wavelength of the ionizing laser is variable in the range of $\lambda_{ion} = 447 \sim 478.8$ nm, corresponding to initial electron temperature in the range of $T_e = 1295 \sim 11.2$ K[29]. The radial directions x , y , and axial direction z of the ion cloud were 2.7, 2.7, and 25.2 mm, respectively [7]. The well-depth of the ion trap was approximately 0.7 eV, corresponding to a maximum temperature ranging at $10^3 - 10^4$ K for the trapped Rb^+ -ion [7, 30]. For the ions created in the photoionization of cold atoms, momentum and energy conservation ensured that the initial kinetic energy of the Rb^+ was approximately two orders of magnitude larger than that of the cold atom[31], that is, 20 mK, which were subsequently heated by disorder-induced heating [29, 32]. As for a typical ultracold neutral plasmas created by photoionizing laser-cooled atoms near the ionization threshold, the effective ion temperature evolved to several 1 K on the timescale of $\sim 10^2$ ns [32], thus the minimum collision energy was approximately 10 mK-K.

Through modelling experimental processes, we had established a rate-equation model. Based on Langevin capture theory[26], two reaction products are considered in our rate-equation model: Rb_2^+ molecular ions as the product of Rb-Rb^+ reaction and Rb_3^+ molecular ions as the product of Rb-Rb_2^+ reaction. As shown in Fig.2, our rate-equation model was well fit the evolution of numbers of ions during the photoionization. Accordingly, rate coefficients including Γ_{diff} , k_2 , k_{23} , $\Gamma_{i-e-recom}$ and $\Gamma_{m-e-recom}$, etc. were derived. We have obtained rate coefficients under different experimental conditions by changing the system parameters, e.g., intensity and wavelength of the ionizing laser. The results are discussed below.

1 Ion-diffusion rate

The measured ion diffusion rate Γ_{diff} . under different system parameters are shown in Fig.3. Generally, Γ_{diff} . falls in the range of Γ_{diff} . $=(0.4\sim 2.0)/s$. Γ_{diff} . is larger when the wavelength of ionizing laser is λ_{ion} . $=478.8$ nm (corresponding to $T_e \approx 11$ K) but is generally independent of intensity of the ionizing laser. Moreover, our measured ion diffusion rate Γ_{diff} . is much lower than the ion diffusion rate of $\sim 1000/s$ in an ultracold neutral plasma (UNP)[32, 33] but higher than a $\sim 0.02/s$ diffusion rate of hot Cs^+ ions[34]. In UNPs, the diffusion of ions are strongly driven by electron pressure due to strong ion-electron spatial correlation[32, 33]. Our Γ_{diff} . manifests that the diffusion of our ions is still affected by ion-electron spatial correlations although no plasma was created, which agrees with our other studies[29]. When the the wavelength of ionizing laser is longer and initial electron temperature is lower, the ion-electron correlations becomes stronger and therefore ions will diffuse faster.

2 Rb-Rb^+ and Rb-Rb_2^+ reaction-rate coefficient

We firstly discuss the result of Rb-Rb^+ reaction-rate coefficient k_2 . The measured k_2 with different system parameters is shown in Fig.4. Obviously, k_2 is independent of system parameters and has a mean value of $(3.32\pm 1.71) \times 10^{-11}$ cm^3/s . This generally agrees with the prediction of Langevin capture theory[13, 26], which estimated that two-body ion-atom reaction-rate coefficient is independent of experimental conditions[26] and falls in the range of $10^{-10} \sim 10^{-12}$ cm^3/s [13].

We now discuss our results on Rb_3^+ produced by Rb-Rb_2^+ reaction and its reaction-rate coefficient k_{23} . Through fitting the experimental data of molecular mixture, we roughly obtained a Rb-Rb_2^+ reaction-rate coefficient of $k_{23} \sim 0.3 \times 10^{-11}$ cm^3/s , which is $\sim 1/10$ of measured k_2 and significantly smaller than the prediction of $k_{23} : k_2 \sim \sqrt{2} : \sqrt{3}$ of Langevin theory[26]. Interestingly, Perez-Rios[14] theoretically investigated Rb-RbBa^+ reactive collisions and reported that when the collisional energy is larger than 10 mK and the molecular ions are in shallower vibrational states, reaction-rate coefficients start to deviate from the Langevin model. Similar results were also observed in the experimental investigation of reactive collisions between Rb and N_2^+ ,

O_2^+ by Dorfler *et al.*[35]. Their results further revealed that the molecular ion-atom reaction-rate coefficient significantly smaller than Langevin model because long-range Langevin-capture model cannot explain the complex short-range dynamics and its effect on molecular ion-atom collisions, especially when the reaction complex has a high internal energy. Considering that our minimum collisional energy is 10 mK-K and Rb_2^+ may not be in deeply bounded vibrational states (see discussions in Sec3), it's reasonable to believe the mechanisms discussed above are probably responsible for the deviation of our result on k_{23} from the Langevin model.

3 Lifetime of the products and affecting mechanisms

As shown in Fig.1, the amount of Rb_2^+ and Rb_3^+ in ionic mixture remained high if Rb^+ were heated and escaped from the mixture, indicating the dissociation of Rb_2^+ and Rb_3^+ is mainly resulted from inelastic collisions with Rb^+ . However, these inelastic collisions between Rb^+ and Rb_2^+ , Rb_3^+ offered us an insight of the quantum state of molecular ions by measuring their dissociation lifetime because the dissociation lifetime of a molecular ion is inherently linked to its quantum state.

We firstly discuss the lifetime of Rb_3^+ . Through fitting the experimental data with rate equations, we have obtained dissociation rate of Rb_3^+ , e.g., Γ_{3m} , which is resulted in the range of (2.0~6.0)/s, corresponding to a remarkably short lifetime of few 100 ms. Our result differs from a recent theoretical study by Smialkowski *et al.*[12], whose results predicted that Rb_3^+ may have a long lifetime because it can enter a very deeply bounded state. We believe our produced Rb_3^+ probably has a different geometric structure from the Rb_3^+ in Ref.[12] and therefore the lifetime of Rb_3^+ is much shorter than their prediction.

Considering that the produced Rb_3^+ is very short-lived, our measured lifetime of molecular mixture actually reveals the lifetime of Rb_2^+ . In this case, the evolution of dissociation lifetime τ_m of Rb_2^+ during photoionization is shown in Fig.5. Specifically, Fig.5(a) has demonstrated that when the intensity of ionizing laser is lower, Rb_2^+ tends to have a longer τ_m and the density of remaining atoms is higher after a same duration of photoionization. This is probably because Rb_2^+ could enter deeply bounded vibrational states via collisions with Rb atoms[14, 36]. With a lower intensity of ionizing laser, the density of atoms remained higher after a same duration of photoionization. Therefore, atom-molecular ion collisions is much more than in the case with higher intensity of ionizing laser and vibrational quenching effect of Rb_2^+ is much observable.

Fig.5 also shown that the dissociation lifetime of Rb_2^+ is oscillating during photoionization. In order to underly the physics of this phenomenon, we studied the relationship between the kinetic energy of Rb_2^+ (represented by width of the TOF peak corresponding to Rb_2^+ [8], narrower peak related to higher kinetic energy) and its dissociation lifetime, as shown in Fig.5(b). Interestingly, we found that when the Rb_2^+ has a shorter dissociation lifetime when

its kinetic energy is higher. This is essentially because when the collisional energy $E_{col} = E_k(\text{Rb}_2^+) + E_{vib.}(\text{Rb}_2^+)$ [37] is higher, both translational energy and internal energy of Rb_2^+ are higher, resulting a shorter dissociation lifetime. However, $E_{vib.}(\text{Rb}_2^+)$ can be converted into $E_k(\text{Rb}_2^+)$ due to the quenching effect from $\text{Rb}-\text{Rb}_2^+$ collisions. In this case, the lifetime of Rb_2^+ is affected by two competing mechanisms. The competition between these two effects is probably responsible for observed oscillating of Rb_2^+ dissociation lifetime during the photoionization.

4 Temperature relaxation of the ionic mixture

Considering Rb_3^+ is low-yielded and short-lived, it actually hardly affect the temperature of Rb^+ and Rb_2^+ . Thus we only investigate temperature relaxation between Rb^+ and Rb_2^+ . Fig.6 presents temperature evolution of Rb^+ and Rb_2^+ mixture during the photoionization. From the result we can notice that there is a strong connection between the temperature of Rb^+ and Rb_2^+ . Specifically, when the photoionization started, temperature of Rb_2^+ increases as temperature of Rb^+ decreases in a short period. Then temperature of Rb_2^+ reaches maximum as temperature of Rb^+ reaches minimum. After that temperature of Rb_2^+ decreases as temperature of Rb^+ increases but they both varies at a slower rate. And this procedure is reversed again and evolves at a much slower rate after $t = 8000$ ms. Eventually, the temperature of two species gradually reaches equilibrium.

This process of reaching thermal equilibrium is similar to that in a dual-species ultracold neutral plasma[38] but has a long duration of over 8000 ms compared to the few μs in UNPs. This suggests that similar ion transportation properties exists in our ionic mixture created by photoionization. As long as we were using an ion trap, no plasma was created because the ion trap strongly repels electrons. This slower equilibrium process allows for simpler and much precise control of the ion mass ratio. And establishes the use of dual-species Coulomb mixture as a unique platform for studying ion transport properties even studying plasmas.

5 CONCLUSIONS

In summary, we studied the kinetics of ion-atom reactive collisions and its dynamics in cw-laser photoionization of laser-cooled ^{87}Rb atoms in an ion-atom hybrid trap. Through precisely controlling the start-stop of reactive collisions and directly measuring ion TOF spectrum, we reported the first direct observation of Rb_3^+ molecular ions. And the evolution of yield, temperature and lifetime of reaction products Rb_2^+ and Rb_3^+ were also obtained. Then, we had modelled the experiments to establish rate-equation model for the number of reactants Rb^+ ions and product Rb_2^+ , Rb_3^+ molecular ions. Simulation of evolution of number of Rb^+ , Rb_2^+ and Rb_3^+ during photoionization provides two-body $\text{Rb}-\text{Rb}^+$ and $\text{Rb}-\text{Rb}_2^+$ reaction-rate coefficients and ion diffusion rate and other physical quantities. The measure ion diffusion rate has proved

that ion-electron spatial correlations would presence during the photoionization even no plasma created (see Fig.3). Our measured Rb-Rb⁺ reaction-rate coefficient well matches the prediction of classical Langevin theory[13, 26] and is independent of system parameters (see Fig.4). Rb-Rb₂⁺ reaction-rate coefficient is smaller than Langevin prediction due to relatively high collisional energy (≥ 10 mK) and Rb₂⁺ is in relatively shallow vibrational states, verifying the observation of short-range dynamics[35]. Besides, we had measured on the variation of quantum state of reaction products during photoionization and reactive collision. The dissociation of bounded Rb₂⁺, Rb₃⁺ mainly results from inelastic collisions with Rb⁺. Our results demonstrated that the quantum state/lifetime of Rb₂⁺ could be affected by two competing mechanisms: vibrational quenching effect due to Rb-Rb₂⁺ collisions[14, 36] and increase of collision energy, as shown in Figs.5. Reasonable use with these two processes may enable precise manipulation of molecular ions at state-to-state level. Furthermore, we demonstrates temperature relaxation in the trapped ionic mixture, picturing ion transportation properties in photoionization (see Fig.6). These dynamical processes provides substantial information on subsequent kinetics of products in reactive collisions[23, 24], paving the way for studying subsequent atomic process in ultracold plasmas[33]. Various application such as precision measurement and quantum simulation are also facilitated[13].

6 Figures

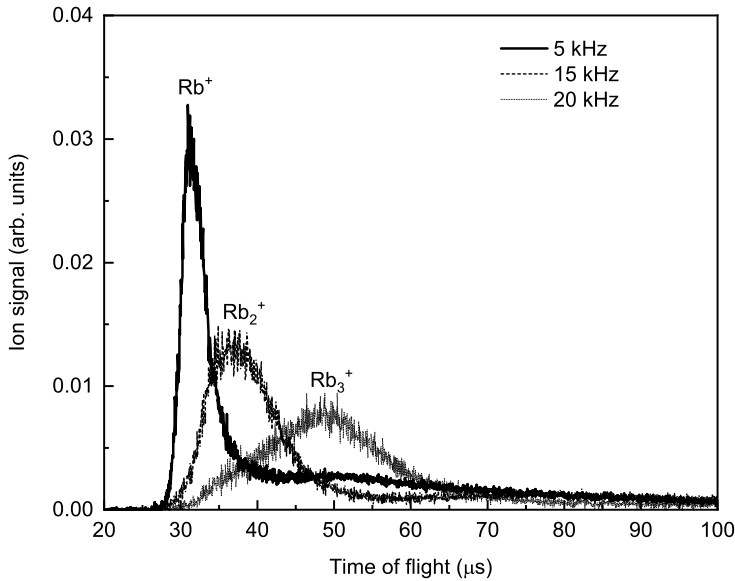


Fig. 1 Ion time-of-flight distribution after a duration of RF heating with different frequency. Data are directly recorded by microchannel plate (MCP) detector after 1500 ms of photoionization duration and 10 ms RF heating duration. Here V_{RF} is set to 4 V. Solid, dashed and dotted lines represents $f_{RF} = 5$ kHz, 15 kHz, 20 kHz, respectively. In this case, system parameters were $\lambda_{ion.} = 478.8$ nm and $I_{PI} = 398$ mW/cm².

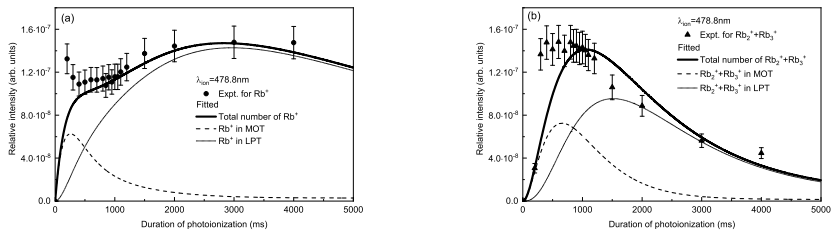


Fig. 2 Ion yield as a function of duration of photoionization. (a) Evolution of the number of Rb^+ . (b) Evolution of the number of $Rb_2^+ + Rb_2^+$ molecular mixture. Solid lines represents total number of Rb^+ or $Rb_2^+ + Rb_2^+$. Dashed lines and dotted lines represents ions in MOT and LPT, respectively. Solid circle and triangle are experimental measured number of Rb^+ or $Rb_2^+ + Rb_2^+$. In this case, system parameters were $\lambda_{ion.} = 478.8$ nm and $I_{PI} = 265$ mW/cm².

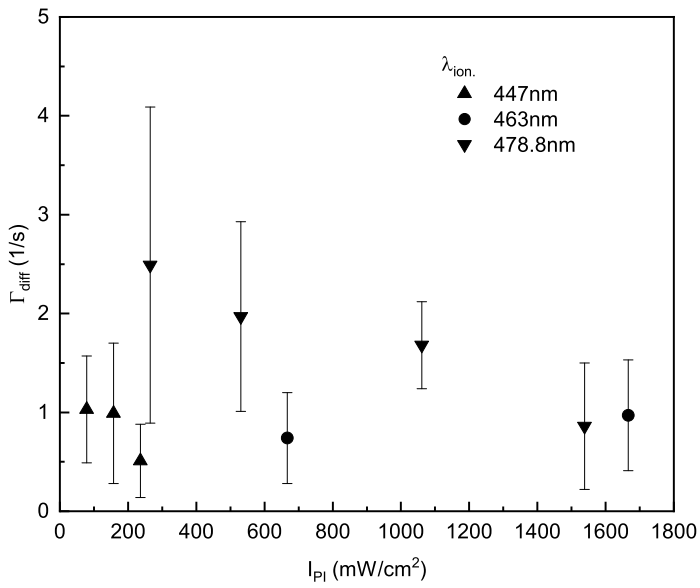


Fig. 3 The diffusion rate of ions in MOT measured with different system parameter. Three wavelength of ionizing laser, i.e., 447 nm (triangle), 463 nm (circle) and 478.8 nm (inversed triangle) were selected to perform the comparison.

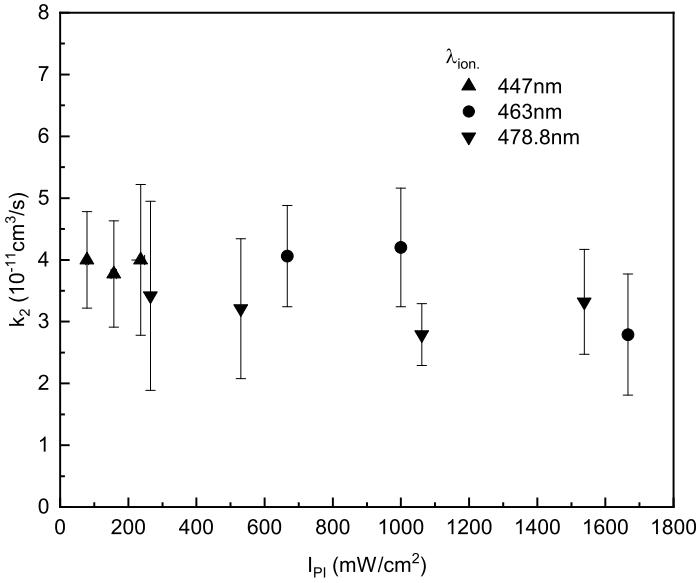


Fig. 4 Rb-Rb⁺ two-body reaction-rate coefficient for of ⁸⁷ Rb measured with different system parameter. Three wavelength of ionizing laser, i.e., 447 nm (triangle), 463 nm (circle) and 478.8 nm (inverted triangle) were selected to perform the comparison. The mean value of measured k_2 is $(3.32 \pm 1.71) \times 10^{-11} \text{ cm}^{-3}$.

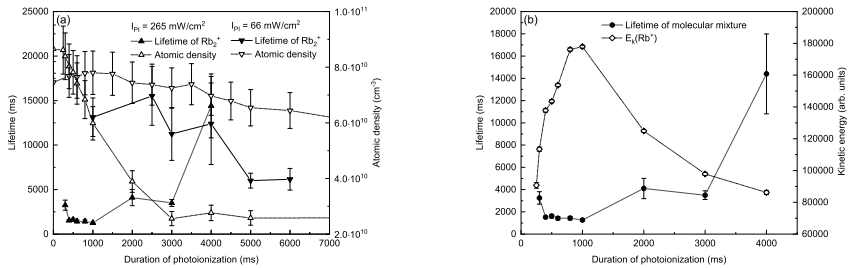


Fig. 5 The evolution of dissociation lifetime of Rb₂⁺ comparing to the evolution of (a) atomic density and (b) kinetic energy of Rb⁺ during the photoionization. In (a), two intensity of ionizing laser were selected. Triangle and inverted triangle respectively stands for the case with $I_{PI} = 265 \text{ mW/cm}^2$ and $I_{PI} = 66 \text{ mW/cm}^2$. Hollows are the density of remaining atoms and solids are lifetime of Rb₂⁺. In (b), hollow diamonds is the kinetic energy of Rb⁺ (in arb. units), which correlates to collision energy. Solid circles are lifetime of Rb₂⁺. The system parameters in (b) were $\lambda_{ion.} = 478.8 \text{ nm}$ and $I_{PI} = 265 \text{ mW/cm}^2$.

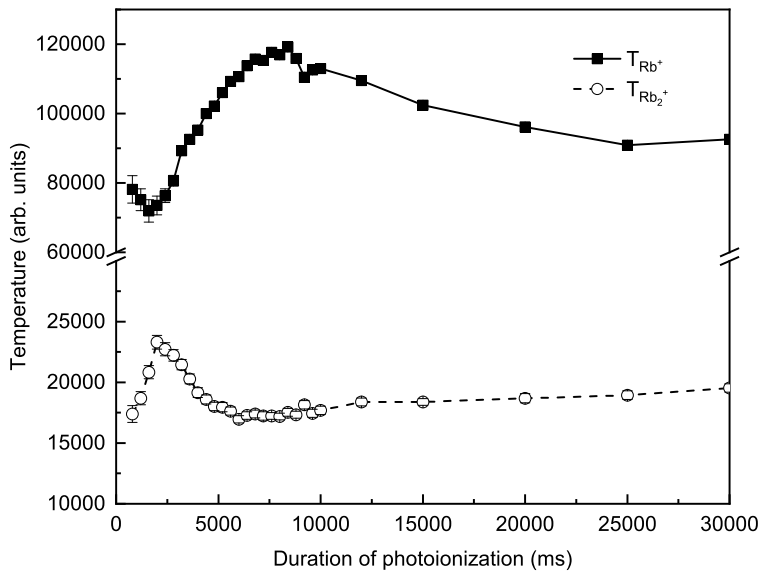


Fig. 6 The evolution of temperature of $\text{Rb}^+ + \text{Rb}_2^+$ mixture during the photoionization. Hollow circles are temperature of Rb_2^+ (in arb. units) and solid squares are temperature of Rb^+ (in arb. units). In this case, system parameters were $\lambda_{ion.} = 447 \text{ nm}$ and $I_{PI} = 19.69 \text{ mW/cm}^2$.

7 Acknowledgments

This study was supported by the National Key Research and Development Program of China (Grant Nos. 2017YFA0402300 and 2017YFA0304900), the Beijing Natural Science Foundation (Grant No. 1212014), the Fundamental Research Funds for the Central Universities, the Key Research Program of the Chinese Academy of Sciences (Grant No. XDPB08-3), specialized research fund for CAS Key Laboratory of Geospace Environment (Grant No. GE2020-01), and National Natural Science Foundation of China (Grant Nos. 61975091, 61575108).

Appendix A Methods

A.1 Rate-equation models

Through modelling the experiments, we have established a rate-equation model to describe the quantity of ions as a function of photoionization duration. Considering energy and momentum conservation, there are two kinds of ion-atom reactive collisions: two-body reaction and three-body reaction[13]. In our experiments, ion-atom three-body reaction was ignored because previous experiments on cold ion-atom three-body reactive collisions[21, 22] occurred in high-density ($\geq 10^{12}\text{cm}^{-3}$) ultracold atoms with collision energies approaching the sub-mK regime. While in our experiments, the atomic density (10^{10} - 10^{11}cm^{-3}) was lower and the minimum collision energy was estimated to 10 mK-K.

Based on Langevin capture theory[26], two reaction products are considered in our rate-equation model: Rb_2^+ molecular ions as the product of Rb-Rb^+ reaction and Rb_3^+ molecular ions as the product of Rb-Rb_2^+ reaction. The ratio of reaction-rate coefficients of Rb-Rb_2^+ to Rb-Rb^+ is estimated to be $\sqrt{2} : \sqrt{3}$ due to $m_{\text{Rb}_2^+} : m_{\text{Rb}^+} = 2 : 1$ [26]. These ions are separated as MOT ions and LPT ions because the density and of ions in LPT ion cloud is much lower than that in MOT ion cloud and the size of LPT ion cloud is much larger than MOT cloud containing ions and atoms, as discussed in Sec.???. As seen in Fig.B1, after a fixed period of photoionizing atoms, the ionizing laser was switched off and LPT was kept on, the yield of reaction products remains unchanged whether the MOT was switched on or off after trapping the ions for a period. This means reactive collision scarcely happens between LPT ions and atoms and only takes place between MOT ions and atoms. In this case, the rate equations for Rb^+ , Rb_2^+ and Rb_3^+ are given as,

$$\begin{aligned} \frac{dN_{ion,MOT}}{dt} = & \gamma_{PI}N_{atom} + \Gamma_m^{diss}N_{mol,MOT} + \Gamma_{3m}N_{3mol,MOT} \\ & - \Gamma_{diff,ion}N_{ion,MOT} - k_2n_{atom}N_{ion,MOT} \\ & - (\Gamma_{trap} + \Gamma_{i-e-recom})N_{ion,MOT}, \end{aligned} \quad (\text{A1})$$

$$\frac{dN_{ion,LPT}}{dt} = \Gamma_{diff}N_{ion,MOT} + \Gamma_m^{diss}N_{mol,LPT} + \Gamma_{3m}N_{3mol,LPT} - \Gamma_{trap}N_{ion,LPT}, \quad (A2)$$

$$\begin{aligned} \frac{dN_{ion}}{dt} = & \gamma_{PI}N_{atom} + \Gamma_m^{diss}N_{mol} + \Gamma_{3m}N_{3mol} \\ & - \Gamma_{trap}N_{ion} - k_2n_{atom}N_{ion,MOT} - \Gamma_{i-e-recom}N_{ion,MOT}, \end{aligned} \quad (A3)$$

$$\begin{aligned} \frac{dN_{mol,MOT}}{dt} = & k_2n_{atom}N_{ion,MOT} - \Gamma_{diff}N_{mol,MOT} \\ & - (\Gamma_m^{diss} + \Gamma_{trap} + \Gamma_{m-e-recom})N_{mol,MOT} \\ & - k_{23}n_{atom}N_{mol,MOT}, \end{aligned} \quad (A4)$$

$$\frac{dN_{mol,LPT}}{dt} = \Gamma_{diff}N_{mol,MOT} - (\Gamma_m^{diss} + \Gamma_{trap})N_{mol,LPT}, \quad (A5)$$

$$\begin{aligned} \frac{dN_{mol}}{dt} = & k_2n_{atom}N_{ion,MOT} - (\Gamma_m^{diss} + \Gamma_{trap})N_{mol} \\ & - \Gamma_{m-e-recom}N_{mol,MOT} - k_{23}n_{atom}N_{mol,MOT}, \end{aligned} \quad (A6)$$

$$\begin{aligned} \frac{dN_{3mol,MOT}}{dt} = & k_{23}n_{atom}N_{mol,MOT} - \Gamma_{diff}N_{3mol,MOT} \\ & - (\Gamma_{3m} + \Gamma_{trap} + \Gamma_{3recom})N_{3mol,MOT}, \end{aligned} \quad (A7)$$

$$\frac{dN_{3mol,LPT}}{dt} = \Gamma_{diff}N_{3mol,MOT} - (\Gamma_{3m} + \Gamma_{trap})N_{3mol,LPT}, \quad (A8)$$

$$\begin{aligned} \frac{dN_{3mol}}{dt} = & \frac{dN_{3mol,MOT}}{dt} + \frac{dN_{3mol,LPT}}{dt} \\ = & k_{23}n_{atom}N_{mol,MOT} - (\Gamma_{3m} + \Gamma_{trap})N_{3mol} - \Gamma_{3recom}N_{3mol,MOT}, \end{aligned} \quad (A9)$$

Where k_2 and k_{23} is the two-body reaction-rate coefficients for Rb-Rb^+ and Rb-Rb_2^+ , respectively. Γ_{diff} is the diffusion rate of MOT ions. In our experiments, Rb^+ , Rb_2^+ and Rb_3^+ are approximately considered to have a same diffusion rate. $\Gamma_{i-e-recom}$ and $\Gamma_{m-e-recom}$ are the ion-electron recombination-rate coefficient for Rb^+ ions and Rb_2^+ , Rb_3^+ molecular ions, respectively. Γ_m^{diss} and Γ_{3m} are dissociation rate of Rb_2^+ and Rb_3^+ (whose dissociation product is considered as a Rb^+). These rate coefficients be discussed later. In these equations, the evolution of number and density of atoms are expressed as $N_{atom}(t) = Ae^{-\gamma_x t} + N_e$ and $n_{atom}(t) = \frac{3N_{atom}(t)}{4\pi \times r_{atom}(t)^3}$, respectively, where $r_{atom}(t) = Be^{-\gamma_r t} + r_e$ [29, 39].

Γ_{trap} is the loss rate of ions in the RF ion trap due to limited trapping capability. In our model, we had assumed a same trapping lifetime for Rb^+ ,

Rb_2^+ and Rb_3^+ due to the fact that the total number of ions $N_{total} = N_{ion} + N_{mol} + N_{3mol}$ follows a single exponential decay as the ions are trapped in the ion trap without the existence of atoms and the ionizing laser.

Due to the limitation of our experimental apparatus, our measured yield of reaction products, e.g., molecular ions is a mixture of Rb_2^+ and Rb_3^+ (mostly are Rb_2^+). Therefore, rate equations for this molecular mixture is written as

$$\begin{aligned} \frac{dN_{totmol,MOT}}{dt} &= \frac{dN_{mol,MOT}}{dt} + \frac{dN_{3mol,MOT}}{dt} \\ &= k_2 n_{atom} N_{ion,MOT} - \Gamma_{diff} N_{totmol,MOT} \\ &\quad - (\Gamma_{trap} + \Gamma_{m-e-recom}) N_{totmol,MOT} \\ &\quad - \Gamma_m^{diss} N_{mol,MOT} - \Gamma_{3m} N_{3mol,MOT}, \end{aligned} \quad (\text{A10})$$

$$\begin{aligned} \frac{dN_{totmol,LPT}}{dt} &= \frac{dN_{mol,LPT}}{dt} + \frac{dN_{3mol,LPT}}{dt} \\ &= \Gamma_{diff} N_{totmol,MOT} - \Gamma_{trap} N_{totmol,LPT} \\ &\quad - \Gamma_m^{diss} N_{mol,LPT} - \Gamma_{3m} N_{3mol,LPT}, \end{aligned} \quad (\text{A11})$$

$$\begin{aligned} \frac{dN_{totmol}}{dt} &= \frac{dN_{mol}}{dt} + \frac{dN_{3mol}}{dt} \\ &= k_2 n_{atom} N_{ion,MOT} - \Gamma_{trap} N_{totmol} \\ &\quad - \Gamma_m^{diss} N_{mol} - \Gamma_{3m} N_{3mol} - \Gamma_{m-e-recom} N_{totmol,MOT}, \end{aligned} \quad (\text{A12})$$

A.2 Measurement of ions

Although suitable operating parameters for Rb^+ ions differ from those for Rb_2^+ molecular ions, we optimized the operating parameters of the LPT to reach a balance where both ions are stabilized, thus both ions were co-trapped in the LPT with reasonable lifetime. Under the assumption that $\Gamma_{trap,mol} \sim \Gamma_{trap,ion} = \Gamma_{trap}$, the decay for either Rb_2^+ molecular ions or total ions at $n_e = n_{atom} = 0$ obeys an exponential decay function. Experimentally, $n_e = n_{atom} = 0$ can be realized by switching off the ionization laser and MOT. As shown in Fig.B2, the observed decay for either $\text{Rb}_2^+ + \text{Rb}_3^+$ molecular mixture or total ions obeys a simple exponential decay formula. Therefore, the assumption $\Gamma_{trap,mol} \sim \Gamma_{trap,ion} = \Gamma_{trap}$ is valid in this work.

A.3 The effect of MOT cooling light on molecular ions

In our experiments, we assumed Γ_m^{diss} is not affected by atoms or MOT cooling light. This was based on the fact that the dissociation rate Γ_m^{diss} of Rb_2^+ is not affected by the presence of MOT cooling light, as seen in Fig.B3. However, Jyothi *et al.*[40] reported that the dissociation lifetime of $^{85}\text{Rb}_2^+$ molecular ions was 16 ± 8 s without the MOT cooling light but dramatically decreased to 495 ± 80 ms with the presence of MOT cooling light. In our experiment, the dissociation lifetime of Rb_2^+ is about 2-3 s, which may be resulted from

that the size of our ion cloud in ion trap is much larger than that in Ref.[40]. As a result, less number of Rb_2^+ are exposed in the MOT cooling beam and the dissociation lifetime/rate roughly remain unaffected, indicating that our apparatus can create a large ensemble of trapped and relatively long-lived Rb_2^+ .

Appendix B Figures

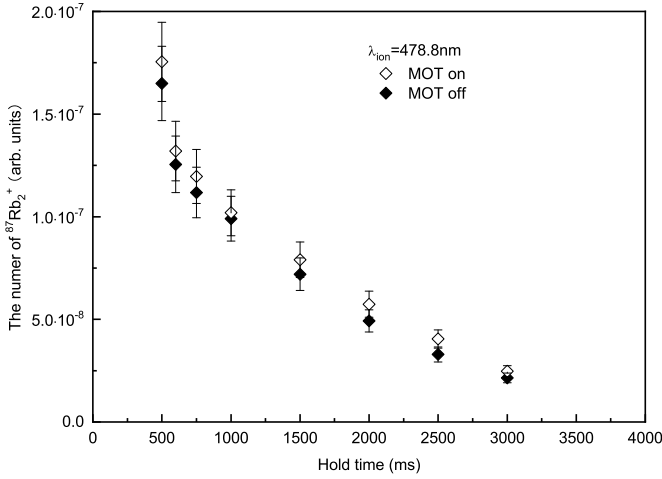


Fig. B1 $^{87}\text{Rb}_2^+$ signal is measured as a function of the hold time in the ion trap with/without presence of cold atoms by switching MOT on or off. The time zero is set to the moment when the ionization laser, gradient magnetic field, and re-pump light are turned off. In this case, system parameters were $\lambda_{\text{ion}} = 478.8 \text{ nm}$ and $I_{\text{PI}} = 265 \text{ mW/cm}^2$.

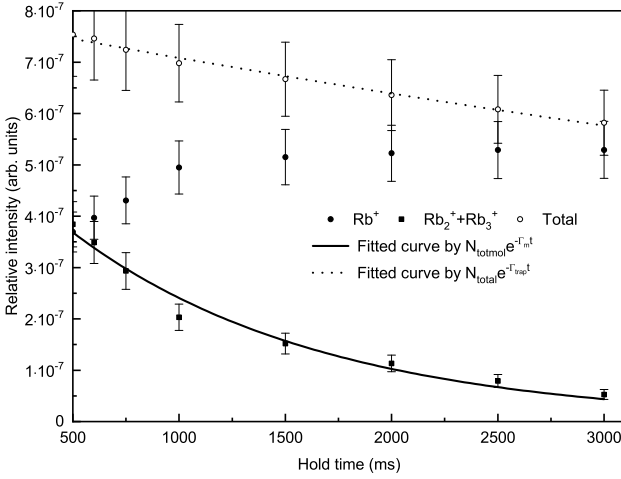


Fig. B2 Rb^+ , $\text{Rb}_2^+ + \text{Rb}_3^+$ and total number of ions as a function of the hold time in the ion trap without cold atoms and the ionizing laser. The time zero is set to the moment that both of the ionizing light and MOT turn off. In this case, system parameters were $\lambda_{\text{ion.}} = 447 \text{ nm}$ and $I_{\text{PI}} = 157 \text{ mW/cm}^2$.

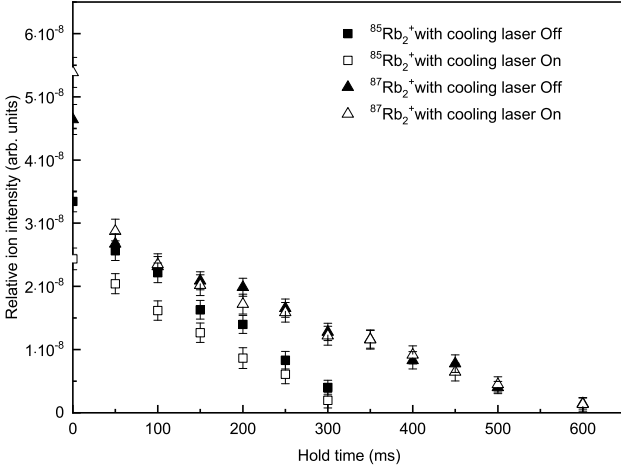


Fig. B3 $^{87}\text{Rb}_2^+$ and $^{85}\text{Rb}_2^+$ signals are measured as a function of the hold time in the ion trap with/without presence of gradient magnetic field, re-pump light and the cooling light. The time zero is set to the moment when the ionization laser is turned off. In this case, system parameters were $\lambda_{\text{ion.}} = 447 \text{ nm}$ and $I_{\text{PI}} = 157 \text{ mW/cm}^2$.

References

- [1] Hall, F.H.J., Aymar, M., Raoult, M., Dulieu, O., Willitsch, S.: Light-assisted cold chemical reactions of barium ions with rubidium atoms. *Molecular Physics* **111**(12-13), 1683–1690 (2013). <https://doi.org/10.1080/00268976.2013.770930>. Accessed 2022-11-06
- [2] Rellergert, W.G., Sullivan, S.T., Kotochigova, S., Petrov, A., Chen, K., Schowalter, S.J., Hudson, E.R.: Measurement of a Large Chemical Reaction Rate between Ultracold Closed-Shell Ca 40 Atoms and Open-Shell Yb + 174 Ions Held in a Hybrid Atom-Ion Trap. *Physical Review Letters* **107**(24), 243201 (2011). <https://doi.org/10.1103/PhysRevLett.107.243201>. Accessed 2022-11-06
- [3] Dulieu, O., Osterwalder, A.: Cold Chemistry: Molecular Scattering and Reactivity Near Absolute Zero. The Royal Society of Chemistry, ??? (2017). <https://doi.org/10.1039/9781782626800>. <https://doi.org/10.1039/9781782626800>
- [4] Ratschbacher, L., Zipkes, C., Sias, C., Khl, M.: Controlling chemical reactions of a single particle. *Nature Physics* **8**(9), 649–652 (2012). <https://doi.org/10.1038/nphys2373>. Accessed 2023-03-17
- [5] Sikorsky, T., Meir, Z., Ben-shlomi, R., Akerman, N., Ozeri, R.: Spin-controlled atomion chemistry. *Nature Communications* **9**(1), 920 (2018). <https://doi.org/10.1038/s41467-018-03373-y>. Accessed 2023-03-17
- [6] Beyer, M., Merkt, F.: Half-Collision Approach to Cold Chemistry: Shape Resonances, Elastic Scattering, and Radiative Association in the H + + H and D + + D Collision Systems. *Physical Review X* **8**(3), 031085 (2018). <https://doi.org/10.1103/PhysRevX.8.031085>. Accessed 2023-03-17
- [7] Lv, S.-F., Jia, F.-D., Liu, J.-Y., Xu, X.-Y., Xue, P., Zhong, Z.-P.: Measurement of the Low-Energy Rb + Rb Total Collision Rate in an Ion-Neutral Hybrid Trap. *Chinese Physics Letters* **34**(1), 013401 (2017). <https://doi.org/10.1088/0256-307X/34/1/013401>. Accessed 2022-11-05
- [8] Liang, W.-C., Wang, Y.-H., Zhang, X., Wang, F., Jia, F.-D., Xue, P., Zhong, Z.-P.: Analysis and simulation of the time-of-flight spectrum in a rb⁺-rb hybrid trap. *Acta Physica Sinica* (accepted) **0**(0), 0 (2023)
- [9] Puri, P., Mills, M., Simbotin, I., Montgomery, J.A., Ct, R., Schneider, C., Suits, A.G., Hudson, E.R.: Reaction blockading in a reaction between an excited atom and a charged molecule at low collision energy. *Nature Chemistry* **11**(7), 615–621 (2019). <https://doi.org/10.1038/s41557-019-0264-3>. Accessed 2022-11-06

- [10] Schowalter, S.J., Chen, K., Rellergert, W.G., Sullivan, S.T., Hudson, E.R.: An integrated ion trap and time-of-flight mass spectrometer for chemical and photo- reaction dynamics studies. *Review of Scientific Instruments* **83**(4), 043103 (2012). <https://doi.org/10.1063/1.3700216>. Accessed 2023-03-17
- [11] Gonzalez-Lezana, T., Honvault, P.: The $H^+ + H_2$ reaction. *International Reviews in Physical Chemistry* **33**(3), 371–395 (2014). <https://doi.org/10.1080/0144235X.2014.943470>. Accessed 2023-03-17
- [12] miakowski, M., Tomza, M.: Interactions and chemical reactions in ionic alkali-metal and alkaline-earth-metal diatomic $A B^+$ and triatomic $A_2 B^+$ systems. *Physical Review A* **101**(1), 012501 (2020). <https://doi.org/10.1103/PhysRevA.101.012501>. Accessed 2023-03-07
- [13] Tomza, M., Jachymski, K., Gerritsma, R., Negretti, A., Calarco, T., Idziaszek, Z., Julienne, P.S.: Cold hybrid ion-atom systems. *Reviews of Modern Physics* **91**(3), 035001 (2019). <https://doi.org/10.1103/RevModPhys.91.035001>. Accessed 2022-11-06
- [14] Prez-Ros, J.: Vibrational quenching and reactive processes of weakly bound molecular ions colliding with atoms at cold temperatures. *Physical Review A* **99**(2), 022707 (2019). <https://doi.org/10.1103/PhysRevA.99.022707>. Accessed 2023-01-31
- [15] Heazlewood, B.R., Softley, T.P.: Towards chemistry at absolute zero. *Nature Reviews Chemistry* **5**(2), 125–140 (2021). <https://doi.org/10.1038/s41570-020-00239-0>. Accessed 2022-11-06
- [16] Dieterle, T., Berngruber, M., Hlzl, C., Lw, R., Jachymski, K., Pfau, T., Meinert, F.: Transport of a Single Cold Ion Immersed in a Bose-Einstein Condensate. *Physical Review Letters* **126**(3), 033401 (2021). <https://doi.org/10.1103/PhysRevLett.126.033401>. Accessed 2022-11-06
- [17] Hall, F.H.J., Aymar, M., Bouloufa-Maafa, N., Dulieu, O., Willitsch, S.: Light-Assisted Ion-Neutral Reactive Processes in the Cold Regime: Radiative Molecule Formation versus Charge Exchange. *Physical Review Letters* **107**(24), 243202 (2011). <https://doi.org/10.1103/PhysRevLett.107.243202>. Accessed 2022-11-06
- [18] Hall, F.H.J., Eberle, P., Hegi, G., Raoult, M., Aymar, M., Dulieu, O., Willitsch, S.: Ion-neutral chemistry at ultralow energies: Dynamics of reactive collisions between laser-cooled Ca^+ ions and Rb atoms in an ion-atom hybrid trap. *Molecular Physics* **111**(14-15), 2020–2032 (2013). <https://doi.org/10.1080/00268976.2013.780107>. arXiv:1302.4682 [physics]. Accessed 2022-11-06

- [19] Sullivan, S.T., Rellergert, W.G., Kotochigova, S., Hudson, E.R.: Role of Electronic Excitations in Ground-State-Forbidden Inelastic Collisions Between Ultracold Atoms and Ions. *Physical Review Letters* **109**(22), 223002 (2012). <https://doi.org/10.1103/PhysRevLett.109.223002>. Accessed 2022-11-06
- [20] Hrter, A., Krkow, A., Brunner, A., Schnitzler, W., Schmid, S., Denschlag, J.H.: Single Ion as a Three-Body Reaction Center in an Ultracold Atomic Gas. *Physical Review Letters* **109**(12), 123201 (2012). <https://doi.org/10.1103/PhysRevLett.109.123201>. Accessed 2022-11-06
- [21] Krkow, A., Mohammadi, A., Hrter, A., Denschlag, J.H., Prez-Ros, J., Greene, C.H.: Energy Scaling of Cold Atom-Atom-Ion Three-Body Recombination. *Physical Review Letters* **116**(19), 193201 (2016). <https://doi.org/10.1103/PhysRevLett.116.193201>. Accessed 2022-11-06
- [22] Krkow, A., Mohammadi, A., Hrter, A., Hecker Denschlag, J.: Reactive two-body and three-body collisions of Ba + in an ultracold Rb gas. *Physical Review A* **94**(3), 030701 (2016). <https://doi.org/10.1103/PhysRevA.94.030701>. Accessed 2022-11-06
- [23] Dieterle, T., Berngruber, M., Hlzl, C., Lw, R., Jachymski, K., Pfau, T., Meinert, F.: Inelastic collision dynamics of a single cold ion immersed in a Bose-Einstein condensate. *Physical Review A* **102**(4), 041301 (2020). <https://doi.org/10.1103/PhysRevA.102.041301>. Accessed 2022-11-06
- [24] Mohammadi, A., Krkow, A., Mahdian, A., Dei, M., Prez-Ros, J., da Silva, H., Raoult, M., Dulieu, O., Hecker Denschlag, J.: Life and death of a cold BaRb + molecule inside an ultracold cloud of Rb atoms. *Physical Review Research* **3**(1), 013196 (2021). <https://doi.org/10.1103/PhysRevResearch.3.013196>. Accessed 2022-11-08
- [25] Hu, M.-G., Liu, Y., Grimes, D.D., Lin, Y.-W., Gheorghe, A.H., Vexiau, R., Bouloufa-Maafa, N., Dulieu, O., Rosenband, T., Ni, K.-K.: Direct observation of bimolecular reactions of ultracold KRb molecules. *Science* **366**(6469), 1111–1115 (2019). <https://doi.org/10.1126/science.aay9531>. Accessed 2022-11-24
- [26] Langevin, M.P. *Annales de Chimie et de Physique* **5**, 245 (1905)
- [27] Ravi, K., Lee, S., Sharma, A., Werth, G., Rangwala, S.A.: Combined ion and atom trap for low-temperature ionatom physics. *Applied Physics B* **107**(4), 971–981 (2012). <https://doi.org/10.1007/s00340-011-4726-6>. Accessed 2023-03-17
- [28] Sesko, D.W., Walker, T.G., Wieman, C.E.: Behavior of neutral atoms

- in a spontaneous force trap. *J. Opt. Soc. Am. B* **8**(5), 946–958 (1991). <https://doi.org/10.1364/JOSAB.8.000946>
- [29] Wang, F., Jia, F.-D., Liang, W.-C., Li, X.-K., Wang, Y.-H., Qian, J.-Y., Zhang, D.-C., Wu, Y., Wang, J.-G., Lu, R.-H., Xu, X.-Y., Ruan, Y.-P., Xue, P., Zhong, Z.-P.: Evolution of the number and temperature of the remaining cold atoms in cw-laser photoionization of laser-cooled ⁸⁷Rb atoms. Unpublished manuscript (2023)
- [30] Li, X.-K., Zhang, D.-C., Lv, S.-F., Liu, J.-Y., Jia, F.-D., Wu, Y., Lin, X.-H., Li, R., Xu, X.-Y., Xue, P., Liu, X.-J., Zhong, Z.-P.: The Rb + Rb collision rate in the energy range of 10³–10⁴ K. *Journal of Physics B: Atomic, Molecular and Optical Physics* **53**(21), 219501 (2020). <https://doi.org/10.1088/1361-6455/abb259>. Accessed 2022-11-06
- [31] Ruan, Y.-P., Jia, F.-D., Liu, L.-W., Sun, Z., Huang, W., Xue, P., Xu, X.-Y., Dai, X.-C., Zhong, Z.-P.: Temperature of the Remaining Cold Atoms after Two-Step Photoionization in an ⁸⁷Rb Vapor Cell Magneto-Optical Trap. *Chinese Physics Letters* **31**(7), 073401 (2014). <https://doi.org/10.1088/0256-307X/31/7/073401>. Accessed 2022-11-26
- [32] Killian, T.C., Pattard, T., Pohl, T., Rost, J.M.: Ultracold neutral plasmas. *Physics Reports* **449**(4-5), 77–130 (2007). <https://doi.org/10.1016/j.physrep.2007.04.007>. Accessed 2022-12-07
- [33] Lyon, M., Rolston, S.L.: Ultracold neutral plasmas. *Reports on Progress in Physics* **80**(1), 017001 (2017). <https://doi.org/10.1088/0034-4885/80/1/017001>. Accessed 2022-12-07
- [34] Fuso, F., Ciampini, D., Arimondo, E., Gabbanini, C.: Ion processes in the photoionization of laser cooled alkali atoms. *Optics Communications* **173**(1-6), 223–232 (2000). [https://doi.org/10.1016/S0030-4018\(99\)00609-4](https://doi.org/10.1016/S0030-4018(99)00609-4). Accessed 2022-12-11
- [35] Drfler, A.D., Eberle, P., Koner, D., Tomza, M., Meuwly, M., Willitsch, S.: Long-range versus short-range effects in cold molecular ion-neutral collisions. *Nature Communications* **10**(1), 5429 (2019). <https://doi.org/10.1038/s41467-019-13218-x>. Accessed 2023-03-07
- [36] Jachymski, K., Meinert, F.: Vibrational Quenching of Weakly Bound Cold Molecular Ions Immersed in Their Parent Gas. *Applied Sciences* **10**(7), 2371 (2020). <https://doi.org/10.3390/app10072371>. Accessed 2022-11-06
- [37] He, M.-M., Hu, J., Wu, C.-X., Zhi, Y., Tian, S.X.: Collision-Energy Dependence of the IonMolecule Charge-Exchange Reaction Ar⁺ + CO → Ar + CO⁺. *The Journal of Physical Chemistry A* **124**(17), 3358–3363 (2020). <https://doi.org/10.1021/acs.jpca.0c02047>. Accessed 2023-03-07

- [38] Sprenkle, R.T., Silvestri, L.G., Murillo, M.S., Bergeson, S.D.: Temperature relaxation in strongly-coupled binary ionic mixtures. *Nature Communications* **13**(1), 15 (2022). <https://doi.org/10.1038/s41467-021-27696-5>. Accessed 2022-11-19
- [39] Lee, S., Ravi, K., Rangwala, S.A.: Measurement of collisions between rubidium atoms and optically dark rubidium ions in trapped mixtures. *Physical Review A* **87**(5), 052701 (2013). <https://doi.org/10.1103/PhysRevA.87.052701>. Accessed 2022-11-08
- [40] Jyothi, S., Ray, T., Dutta, S., Allouche, A., Vexiau, R., Dulieu, O., Rangwala, S.: Photodissociation of Trapped $\text{Rb } 2 +$: Implications for Simultaneous Trapping of Atoms and Molecular Ions. *Physical Review Letters* **117**(21), 213002 (2016). <https://doi.org/10.1103/PhysRevLett.117.213002>. Accessed 2022-11-06